Carbohydrate Polymers 92 (2013) 1743–1751

Contents lists available at SciVerse ScienceDirect

Carbohydrate Polymers

journal homepage: www.elsevier.com/locate/carbpol

Brucite nanoplates reinforced starch bionanocomposites

Francys K.V. Moreira [a,b], Daniel C.A. Pedro [a,c], Gregory M. Glenn [d], José M. Marconcini [a], Luiz H.C. Mattoso [a,*]

[a] Laboratório Nacional de Nanotecnologia para o Agronegócio (LNNA), Embrapa Instrumentação (CNPDIA), São Carlos (SP), Brazil
[b] Programa de Pós-graduação em Ciência e Engenharia de Materiais (PPG-CEM), Universidade Federal de São Carlos (UFSCar), São Carlos (SP), Brazil
[c] Departamento de Engenharia de Materiais (DEMA), Universidade Federal de São Carlos (UFSCar), São Carlos (SP), Brazil
[d] Western Regional Research Center (WRRC), Agricultural Research Service (ARS), United States Department of Agriculture (USDA), Albany, CA, United States

ARTICLE INFO

Article history:
Received 30 July 2012
Received in revised form 24 October 2012
Accepted 1 November 2012
Available online 14 November 2012

Keywords:
Biodegradable plastics
Starch
Brucite nanoplates
Bionanocomposites
Mechanical reinforcement

ABSTRACT

In this paper the mechanical reinforcement of nano-sized brucite, $Mg(OH)_2$ in a series of bionanocomposite films based on starch was investigated. Brucite nanoplates with an aspect ratio of 9.25 were synthesized by wet precipitation and incorporated into starch matrices at different concentrations (0–7.5 wt.%). Scanning electron microscopy revealed a high degree of nanoplate dispersion within the starch bionanocomposites and good interfacial adhesion between the filler and matrix. The brucite nanoplates formed agglomerates at high concentrations. The reinforcement factor values of the bionanocomposites were higher than the values predicted from the Halphin–Tsai model, which was attributed mainly to the high surface area of the nanoplates. Brucite (1 wt.%) nearly doubled the elastic modulus of starch films. Thermogravimetric analyses indicated some interaction between starch and the brucite that modified their decomposition profiles. Mechanical tests of glycerol plasticized bionanocomposites showed that the reinforcing efficiency of brucite remained high even at 10 wt.% and 20 wt.% of plasticizer.

1. Introduction

Natural polymers have inspired research aimed at developing new biodegradable plastics for environmentally compatible packaging including single-use commodity materials (Imam, Glenn, Chiou, Shey, & Narayan, 2008). Starch is one of the most widely available and cheap agricultural biopolymers that is being considered for developing these greener technologies (Avérous, 2004; Mitrus, 2009). Starch possesses a structure assembled as semi-crystalline granules composed of two macromolecules, amylose and amylopectin. Amylose is a mostly linear polymer with α-D-(1→4)-linked glucose units while amylopectin is a highly branched polymer comprised of α-D-(1→4) linked glucose units with branches formed by α-D-(1→6) linkages at the branch points.

It has been exhaustively demonstrated that native starch granules can be transformed into biodegradable plastic films by casting of gelatinizated starch solutions or by melt-processing. Both processes employ heat and plasticizers like glycerol to break down the granule structure (Mitrus, 2009). Nevertheless, these biodegradable materials generally exhibit inferior thermal, mechanical and barrier properties compared to petroleum derived plastics, which limits their commercial applications. A promising approach to overcoming these disadvantages in starch films is the use of nano-sized fillers. Nano particles can affect the physical properties of biodegradable polymers even when used in small amounts (<5%) (Ray & Bousmina, 2005).

Bionanocomposites are a new class of nanocomposite materials on the frontier between material science, life science and nanotechnology (Darder, Aranda, & Ruiz-Hitzky, 2007). They can be defined as a combination of a naturally occurring biodegradable polymer (like starch) with an inorganic (or organic) solid that displays at least one dimension in the nanoscale range (Zhao, Torley, & Halley, 2008). When the solid moiety exhibits properties of biomineralization and non-toxicity, the bionanocomposites are also environmentally compatible and can be referred to as a "*green bionanocomposite*". Studies aimed at developing fully biodegradable bionanocomposites often draw from knowledge gained from synthetic polymer-based nanocomposites. In this context, numerous types of nano-sized fillers have been incorporated into starch matrices to improve their physical properties. The most extensive research has focused on layered clay minerals, including kaolinite (De Carvalho, Curvelo, & Agnelli, 2001), sodium and organomodified montmorillonites (Chiou et al., 2007; Chivrac, Pollet, Schmutz,

* Corresponding author at: Laboratório Nacional de Nanotecnologia para o Agronegócio (LNNA), Embrapa Instrumentação (CNPDIA), Rua XV de novembro, 1452, 13560-970 São Carlos (SP), Brazil. Tel.: +55 16 2107 2803; fax: +55 16 2107 2902.
E-mail address: mattoso@cnpdia.embrapa.br (L.H.C. Mattoso).

0144-8617/$ – see front matter © 2012 Elsevier Ltd. All rights reserved.
http://dx.doi.org/10.1016/j.carbpol.2012.11.019

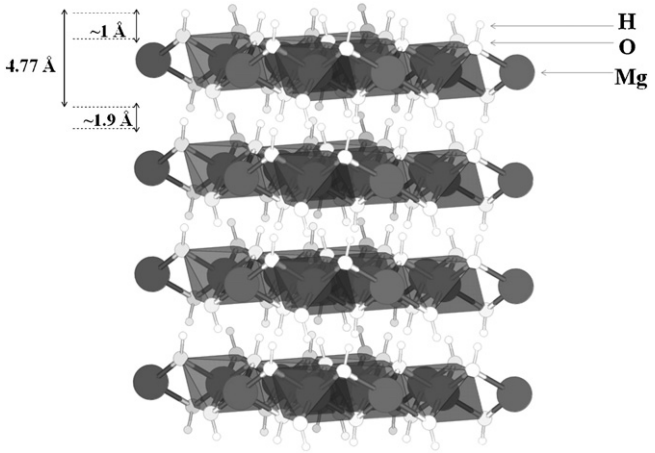

Fig. 1. Crystalline structure of brucite.
Adapted from Brucite Mineral Data in webmineral.com.

& Avérous, 2008), hectorite (Chen & Evans, 2005), sepiolite (Chivrac, Pollet, Schmutz, & Avérous, 2010), Zn–Al layered double hydroxide (Wu, Chang, & Ma, 2011), and rectorite (Chang, Wu, Anderson, & Ma, 2012). To our knowledge, however, the "nano effect" of simple layered minerals like brucite, $Mg(OH)_2$, on the properties of starch films has not been reported.

Brucite is one of the most primitive minerals in the natural clay family. Its structure is based on magnesium ions octahedrally coordinated by hydroxide ions in an electrically neutral lattice (Carrado, 2004). The octahedral units form layers by edge-sharing, such that the hydroxide ions sit perpendicular to the plane of the layers (Fig. 1). The O—H bond length is close to 1 Å while the H—H distance between the layers is approximately 1.9 Å (Baranek, Lichanot, Orlando, & Dovesi, 2001). The symmetry of the brucite lattice is hexagonal and the space group is $P\bar{3}ml$. The interlayer interactions are relatively weak and mainly associated with dispersion forces and hydrogen bonding (Baranek et al., 2001).

There are several methods of synthesizing brucite including homogeneous phase precipitation (He, Wang, Deng, Yin, & Gong, 2008; Henrist, Mathieu, Vogels, Rulmont, & Cloots, 2003), hydrothermal and solvothermal reactions (Ding et al., 2001) and sol–gel techniques (Utamapanya, Klabunde, & Schlup, 1991). All of these methods are effective in forming high purity brucite mineral. By controlling some reaction parameters, the morphological characteristics of brucite can also be tailored to form crystals with useful morphologies such as plates (Jia & Gao, 2006), tubes (Zhuo, Ge, Cao, & Tang, 2009), flowers (Yan, Xue, Zou, Yan, & Wang, 2005) and needles (Ding et al., 2001; Jeevanandam, Mulukutla, Yang, Kwen, & Klabunde, 2007).

Brucite has been used commercially in anti-acids, absorbent pharmaceuticals, water treatment and as an additive in paper products. In recent years, brucite has drawn attention owing to its potential as a non-toxic flame retardant for conventional synthetic polymers (Rothon & Hornsby, 1996). The flame retardancy effect of brucite nanoparticles was investigated recently for poly(ethylene terephthalate) (PET) (Liu, Wang, & Xu, 2010) and isotatic polypropylene (iPP) (Oyama, Sekikawa, & Ikezawa, 2011). These studies demonstrated that the nanocomposites have lower flammability than the pure polymers, but only when substantial amounts of properly dispersed brucite nanoparticles are used.

In the case of starch matrices, brucite nanoparticles may improve thermal stability of composite materials and act as an effective reinforcing filler because of its hydrophilic nature. The filler-matrix adhesion in this system could be enhanced by the presence of hydroxyl groups on the brucite surface that may lead to the formation of hydrogen bonds with starch matrix (Wilhelm, Sierakowski, Souza, & Wypych, 2003). Furthermore, brucite is generally recognized as safe (GRAS, no. 1309-42-8) according to the Food and Drug Administration (FDA, USA) and the Agência Nacional de Vigilância Sanitária (Anvisa, Brazil). These unique properties make nanocomposites of starch and brucite attractive for designing green plastics, especially those intended for food packaging applications.

The present study is aimed at developing bionanocomposite films based on starch and brucite nanoparticles, and determining whether these hybrid materials have improved properties. The microstructure and properties of films were investigated by means of scanning electron microscopy (SEM), wide angle X-ray scattering (WAXS), uniaxial tensile tests and thermogravimetric analyses (TGA). The Halpin–Tsai model was used to examine the reinforcing effect of the brucite nanoparticles on the starch matrix, and whether a "nano-effect" may play a role in the mechanical behavior of the bionanocomposites. The mechanical properties were also examined in films with different levels of glycerol.

2. Materials and methods

2.1. Materials

Native corn starch (~28% amylose and 72% amylopectin) was kindly supplied by Corn Products Brazil Ltda (Campinas, SP). Magnesium chloride, sodium hydroxide, glycerol and other reagents were analytical grade. Deionized water obtained with an ultrapure water purification system (Barnstead Nanopure Diamond™, Thermo Fisher Scientific Inc., USA) was used in all experimental procedures.

2.2. Synthesis of brucite

The nanoparticles of $Mg(OH)_2$ were prepared by homogeneous phase precipitation at 25 °C. Sodium hydroxide (1 mol L^{-1}) was added drop by drop to a Mg^{2+} solution (0.5 mol L^{-1}) using a peristaltic pump operating at an injection rate of 1 mL min^{-1}. Vigorous stirring was applied throughout the entire procedure. Once a precipitate formed, the stirring was continued an additional 1 h to age the sample in the mother liquid. Successive cycles of washing using water and centrifugation (16,770 × *g*) were used to recover the precipitate in a pellet. Afterwards, the pellet was freeze-dried at −80 °C under vacuum at 1.33×10^{-4} bar (Supermodulyo Freeze Dryer, Thermo Fisher Scientific Inc., USA).

2.3. Preparation of bionanocomposite films

Bionanocomposite films were prepared by a casting/evaporation method. In brief, a dilute aqueous starch solution (mass fraction of 0.02) was prepared by disruption of the native starch granules in 180 mL water at 80–85 °C using a mechanical shaker (Turrax MA 102, Marconi, Brazil) working at 12,000 rpm. After 10 min of mixing and cooling to room temperature, aqueous dispersions of brucite (180 mL) were added into the starch solution to yield nanoparticle concentrations of 0.1, 0.25, 0.5, 1.0, 2.5, 5.0 and 7.5 wt.% (dry starch mass basis). Each brucite/starch mixture was plasticized by the addition of 10, 20 and 30 wt.% of glycerol (dry starch mass basis). All compositions were stirred vigorously with a magnetic stirrer for 1 h at room temperature. Finally, the aqueous mixtures were cast in a Teflon mold. The solvent was removed via evaporation in an air circulating oven at 35 ± 2 °C to form thin films of 20–80 μm thickness. The films were equilibrated at 50% (±5%) relative humidity for 48 h prior to testing.

2.4. Characterization

Scanning electron microscopy (SEM). Morphological characterization was performed using a Magellan microscope (FEI Company, Netherlands) running at 1–5 kV and a working distance of between 2 and 3 mm. Cross-sectional views of polymer samples were prepared by freeze-fracturing in a liquid nitrogen bath. All samples were coated with gold (~5 nm) in an argon atmosphere. Nanoparticle samples were prepared by deposition of powders on conductive graphite paint (SPI Supples, USA). All images were recorded using the secondary electron mode.

Wide angle X-ray scattering (WAXS). X-ray scattering experiments were carried out using a diffractometer XRD 6000 (Shimadzu Corporation, Japan) operating with a Cu anode (monochromatizated K_α radiation, $\lambda = 1.541$ Å) excited with a potential of 40 kV and a filament current of 30 mA. Samples were scanned at room temperature over $2\theta = 5–80^\circ$ with a scanning rate of $2^\circ\ min^{-1}$.

Tensile tests. The mechanical properties of the films were determined according to the ASTM D882-09 protocol using a universal testing machine EMIC DL3000 (EMIC Equipamentos e Sistemas de Ensaio LTDA, Brazil) equipped with a 50 kgf load cell. Tests were performed on specimens strips (10 cm × 1 cm) using cross-head speed of 25 mm min^{-1}. Elastic modulus (E) was calculated from the slope of the linear region of the stress–strain curves. Tensile strength and elongation at break were also determined from stress/strain data. Five replicates were performed to define the average properties of each film composition.

Thermogravimetric analyses (TGA). The thermogravimetric (TG) and differential thermogravimetric (DTG) curves were obtained using a thermal analyzer Q500 (TA Instruments, USA). Samples weighing 7–10 mg were heated from 25 °C to 600 °C at a heating rate of 10 °C min^{-1} in a dynamic atmosphere of synthetic air (80% N_2 and 20% O_2) with flow rate of 100 mL min^{-1}. The moisture content of the samples was considered as the mass loss at 150 °C. The onset temperature (T_{onset}), i.e. the temperature at which the polymer degradation starts, was defined at a mass loss of 3% after 150 °C. Inorganic content was determined by the residue left at 600 °C. Two replicates were analyzed for each sample.

3. Results and discussion

3.1. Brucite characterization

Prior to incorporating into starch films, the as-obtained brucite powder was characterized by SEM to verify formation of nano-sized particles (Fig. 2). The electron micrographs revealed nanoparticles with a plate-like morphology and irregular contour (Fig. 2a and b). This morphology was typical of brucite nanoplates due to its hexagonal structure. The brucite nanoplates had diameters ranging from 32 nm to 140 nm (Fig. 2c), and a thickness ranging from 5 to 14 nm (Fig. 2d). The observed morphology of brucite nanoplates was consistent with previous findings using a similar method except that the dimensions here were smaller (An et al., 2009; Henrist et al., 2003). The difference in nanoplate size was probably due to the lower injection rate of the reactant used in this study (1 mL min^{-1} vs. 3 mL min^{-1}). Injection rate is an important parameter that affects the nuclei aggregation and crystal growth in solution (Lv, Qiu, & Qu Baojun, 2004). The average diameter and thickness of the brucite nanoplates were 80.0 ± 23.4 nm and 8.7 ± 1.9 nm, respectively, implying an average diameter to thickness ratio (A_r, aspect ratio) of approximately 9.25.

3.2. Structural aspects of brucite–starch bionanocomposites

WAXS analyses were performed to describe the crystalline phases occurring in brucite–starch bionanocomposite films (Fig. 3). The typical WAXS pattern for these nanoplates exhibited peaks associated with its hexagonal structure (JCPDS indexation no. 7-239) (Fig. 3a). There were no peaks related to other crystalline solid phases, confirming the high degree of purity of the brucite

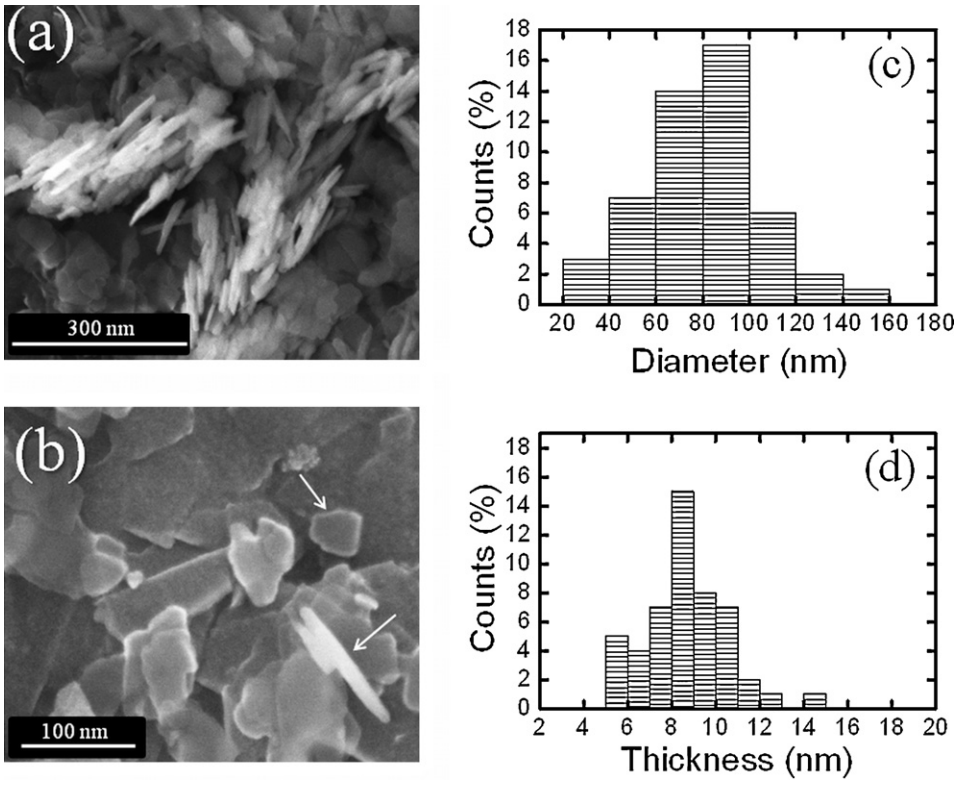

Fig. 2. Characterization of brucite sample. (a and b) High magnification SEM micrographs; (c and d) the diameter and thickness distributions from SEM analyses.

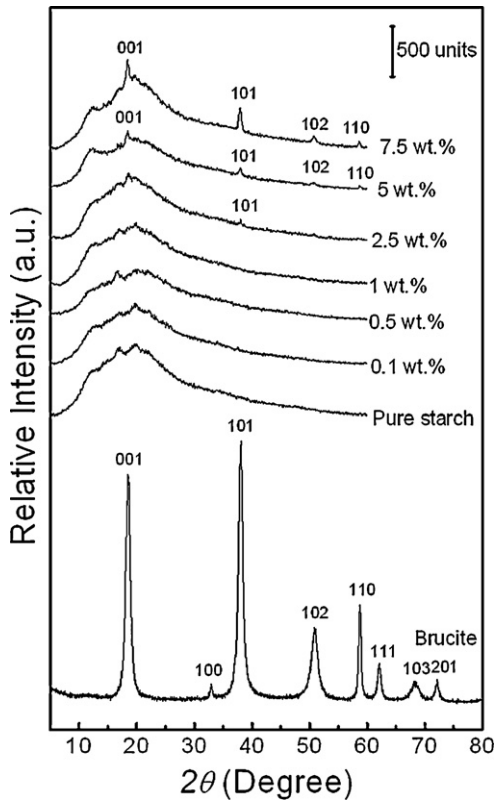

Fig. 3. WAXS patterns for brucite, non-plasticized pure corn starch film and its respective bionanocomposites at different concentrations of brucite nanoplates.

nanoplates. Native corn starch granules exhibited an A-type polymorphism (Corradini et al., 2005), which is characterized by peaks at 14.8°, 16.6°, 17.7° and 22.6° of 2θ (Van Soest, Hulleman, De Wit, & Vliegenthart, 1996). Conversely, the WAXS pattern for pure starch film displayed only a broad peak between 10° and 30° of 2θ with a residual A-type crystallinity identified by the weak peak at 16.6° of 2θ. This result suggested that the granular structure of the corn starch was effectively destroyed in the film-forming process.

Bionanocomposite films exhibited analogous WAXS patterns while scattering peaks from brucite nanoplates were hard to detect. Only film samples containing 5 wt.% and 7.5 wt.% of nanoplates showed peaks characteristic of brucite, as indicated in Fig. 3. This data confirmed the presence of brucite within the starch films. For other compositions, the absence of brucite peaks may be due to the low concentration of the nanoplates.

It is important to point out that although brucite had a layered structure, it did not possess intercalation properties of some clays because its interlayer space was much too short (1.9 Å) to allow penetration of polymer chains or even many smaller molecules. Furthermore, some clays can induce recrystallization of amylopectin at the filler interface through hydrogen bonding. This phenomenon has been recently reported in the case of sepiolite reinforced starch bionanocomposites (Chivrac et al., 2010). Such a recrystallization phenomenon was not observed in the WAXS patterns. Therefore, the brucite–starch bionanocomposite films were characterized as having an amorphous matrix that enveloped the brucite crystals.

Fig. 4a illustrates the macroscopic appearance of some bionanocomposite films. It can be observed that pure starch film and other samples were homogeneous and very transparent which is consistent with the low degree of crystallinity evidenced by WAXS. The findings also indicate that the brucite nanoplates were adequately dispersed in starch matrix. Nevertheless, white aggregates were visible with the incorporation of brucite at higher concentrations. A tenuous haze was observed for films containing 7.5 wt.% brucite (Fig. 4a). This haze is most likely due to excessive quantities of brucite that formed agglomerates, interfering with the light transparency of the bionanocomposite films.

In general, the formation of the bionanocomposites involved a simple blending process wherein brucite was dispersed in the starch solution. The final dispersion level was determined by the amount of shear force imposed during the homogenization step. It was expected that the nanoparticle dispersion would remain unchanged during the film drying process and that a bionanocomposite film would form with dispersed brucite nanoplates interacting with the starch matrix through hydrogen bonding. A proposed structure for the brucite–starch bionanocomposite is schematically illustrated in Fig. 4b.

SEM was performed on cross-sectioned surfaces of the bionanocomposites to verify the degree of brucite nanoplates dispersion. Typical micrographs taken at 1 kV are presented in Fig. 4c–h. The dispersion observed among bionanocomposites containing 0.25 wt.%, 0.5 wt.% and 1 wt.% of brucite was similar (Fig. 4c, d and e, respectively). The micrographs clearly showed individual brucite nanoplates randomly spaced within the polymeric matrix, indicating that a high level of dispersion was reached. There were very few areas where the nanoparticles formed agglomerates and these were penetrated by the starch matrix. The strength of interfacial adhesion was observed by studying the fracture surface of films with 1 wt.% brucite (Fig. 4f). As seen in the micrograph, the brucite nanoplates were imbedded in the starch matrix. The nanoplates appeared to have a thin coating of matrix material rather than fracturing at the matrix/particle interface which is indicative of good adhesion. Well adhered nanoplates and interpenetrated agglomerates may be attributed to the chemical compatibility between starch and brucite, as was expected (Wilhelm et al., 2003). The interfacial bonding may result from hydrogen bonding between hydroxyl groups of the starch macromolecules and the exposed hydroxyl groups on the surface of brucite nanoplates.

At 7.5 wt.% of brucite, larger agglomerates of nanoplates were observed by SEM (Fig. 4g and h). It can be seen that large agglomerates were also internally covered with the starch matrix, indicating that re-agglomeration of nanoplates had occurred even after ultrasonic treatment. This was probably caused by the lack of electrostatic charges in the brucite layers, which was favorable for flocculation behavior in water. The use of dilute starch solution is another important aspect for the resulting morphology. The low viscosities more easily allowed motion in the nanoparticles leading to re-agglomeration during the film-forming process. An increase in volume fraction for randomly arranged particles generally diminishes the average particle separation (Norman & Robertson, 2003). Therefore, an increase in size of the agglomerates can be expected with increasing mass concentration (or volume fraction) of brucite. This could also decrease the effective interfacial area formed between the starch matrix and brucite nanoplates, and influence the mechanical performance of the bionanocomposites as will be discussed hereafter.

3.3. Mechanical performance

Fig. 5 shows the mechanical properties of the non-plasticized starch film with increasing concentration of brucite. The pure starch film exhibited an elastic modulus of 895 MPa, tensile strength of 32 MPa and 5.7% elongation at break. For comparison, an incremental increase both in elastic modulus and tensile strength can be seen for films containing brucite nanoplates (Fig. 5a and b, respectively), whereas there was little effect on elongation (Fig. 5c). This means that an enhancement of the stress level occurred without drastically reducing the energy needed to fracture the starch matrix.

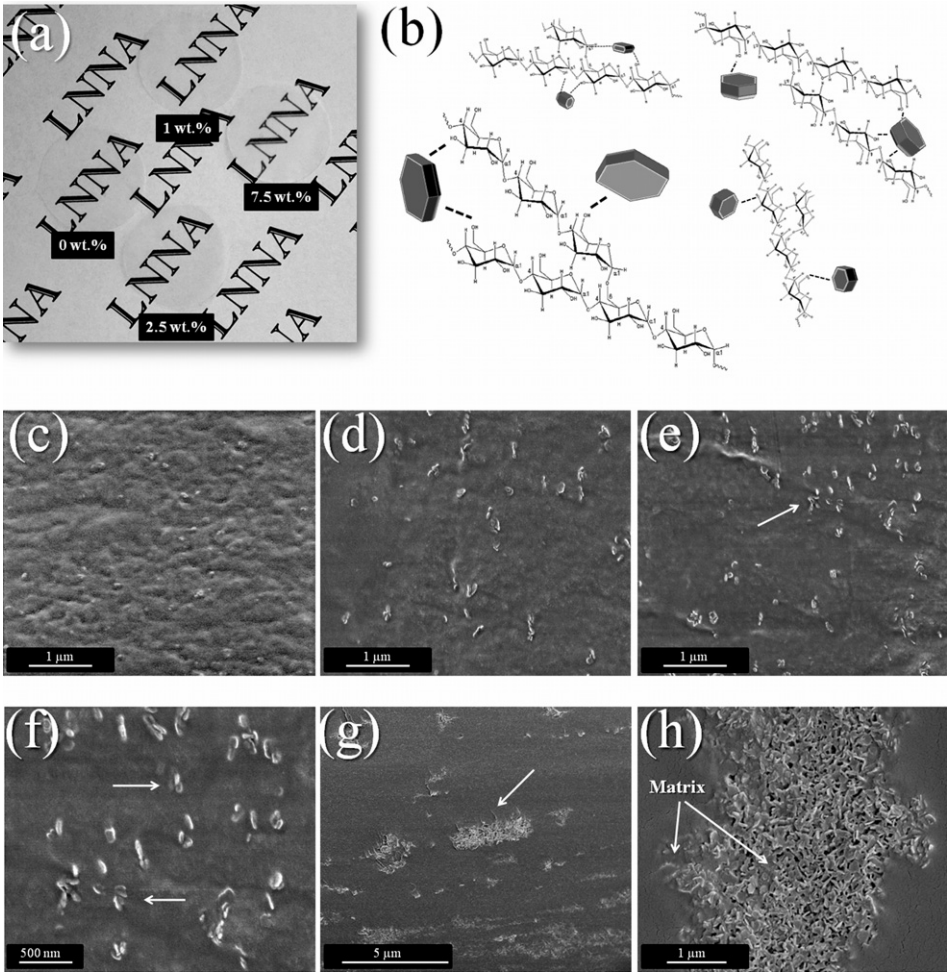

Fig. 4. (a) Transparence of the pure starch films and its bionanocomposites containing 1 wt.%, 2.5 wt.% and 7.5 wt.% of brucite; (b) schematic illustration of the possible interaction of dispersed brucite with the starch polymers comprising the matrix material; (c–e) SEM micrographs cryo-fractured cross sections of bionanocomposites with 0.25 wt.%, 0.5 wt.% and 1 wt.% brucite, respectively; (f) high magnification SEM micrograph cryo-fractured cross sections of 1 wt.% brucite bionanocomposite; (g and h) SEM micrographs cryo-fractured cross sections of 7.5 wt.% of brucite bionanocomposite.

These results provided evidence of stress transfer between starch and brucite nanoplates, and an increased toughness for the bionanocomposites.

The addition of brucite increased the tensile strength of the starch films linearly until reaching approximately 43 MPa at 1 wt.% (region I). Adding higher amounts of brucite did not lead to a further enhancement in tensile strength and a plateau behavior appeared in range 1–7.5 wt.% (region II). Similarly, elastic modulus also increased with increasing concentrations of brucite, but the increment occurred progressively up to 1776 MPa for the 5 wt.% brucite reinforced film. The bionanocomposite film with 7.5 wt.% brucite had properties comparable to those of pure starch film (region III). This was likely due to the excessive amount of agglomerates formed at the 7.5% concentration of brucite. The agglomerates probably behaved as structural defects in the bionanocomposite.

The mechanical reinforcement of the brucite–starch bionanocomposites was examined in a classical manner, relating crystal modulus and geometry of brucite using the Halpin–Tsai equation

$$\frac{E_{\text{composite}}}{E_{\text{matrix}}} = \frac{1 + 2_{A_r} \cdot \mu \cdot \varphi}{1 - \mu \cdot \varphi} \quad (1)$$

where $E_{\text{composite}}/E_{\text{matrix}}$ is the reinforcement factor, A_r is the aspect ratio of the filler (>1 if it is defined as diameter divided by thickness for cylindrical platelets), φ is the volume fraction of filler in the composite, and μ is given by:

$$\mu = \frac{\varepsilon_r - 1}{\varepsilon_r + 2 \cdot A_r} \quad (2)$$

where ε_r is the ratio of the filler to the matrix modulus.

The Halpin–Tsai model was applied to predict the modulus of composite materials where one assumes completely dispersed particles and a perfect adhesion between filler and matrix (Halpin & Kardos, 1972, 1976). As revealed by SEM results, the brucite nanoplates can form agglomerates during the film-forming process. This means that the Halpin–Tsai model was just an idealized approach for studying the brucite–starch bionanocomposites, and may be regarded as the potential upper limit for mechanical reinforcement. Another important aspect to be considered is that in the case brucite there is a remarkably mechanical anisotropy regarding the crystallographic direction in the crystal. This effect was related to the layered structure in which the chemical bonds between and along the layers are different. Some elastic moduli of brucite have been experimentally calculated and found to be 156 GPa (parallel to layer), 46 GPa (normal to layer) while the shear modulus was around 30.4 GPa (Xia, Weidner, & Zhao, 1998). The parallel and normal elastic constants were used in the Halpin–Tsai approach to predict the reinforcement efficiency of brucite in starch bionanocomposites and further compare them with the experimental

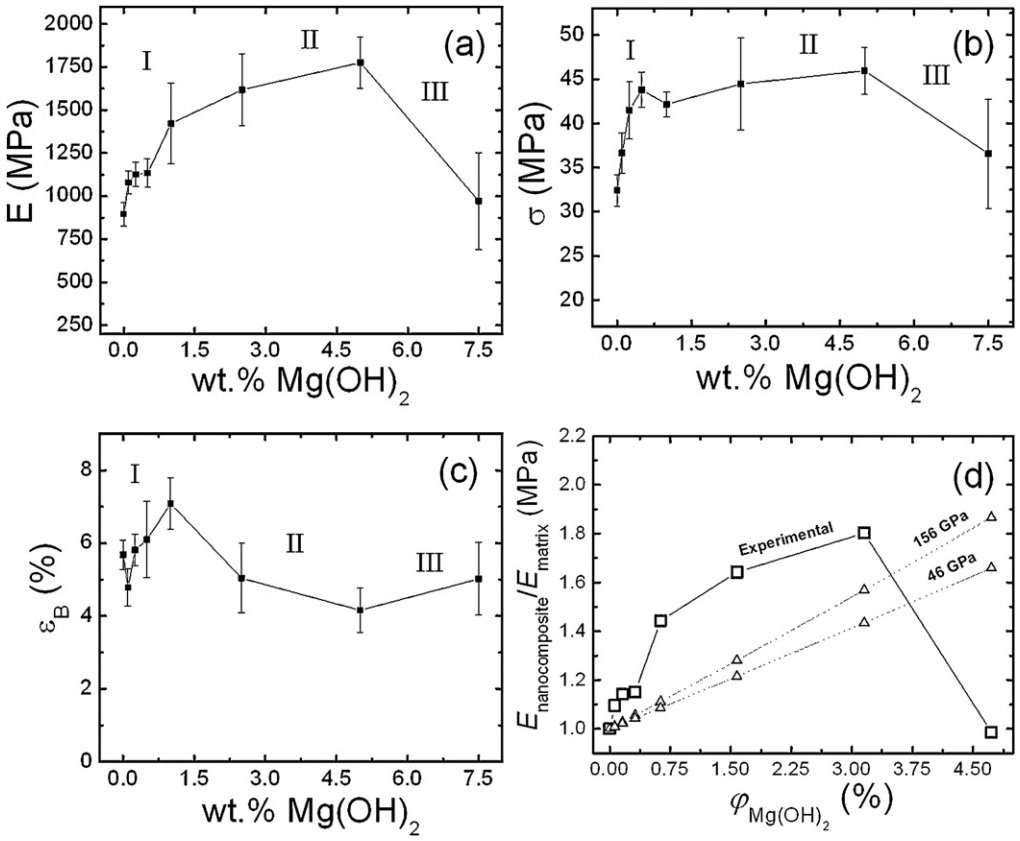

Fig. 5. Tensile mechanical properties of the non-plasticized starch films vs. brucite concentration. (a) Elastic modulus, (b) tensile strength, (c) elongation at break, and (d) $E_{nanocomposite}/E_{matrix}$ vs. brucite volume fraction for brucite–starch bionanocomposite films. (Linear lines are fits from the classical Halpin–Tsai model generated using elastic modulus along the layer direction, 156 GPa, and bulk modulus, 46 GPa, of brucite. Data used for fitting: $A_r = 9.25$; $\rho_{brucite} = 2.379\,g\,cm^{-3}$ (Xia et al., 1998); $\rho_{starch} = 1.5\,g\,cm^{-3}$ (Zhao, 1998)).

results. The curves were plotted as a function of the brucite volume fraction, as displayed in Fig. 5d.

The increase in the experimental reinforcement factor deviated to values higher than the Halphin–Tsai predictions, even when the highest crystal modulus was considered. This meant that the tensile properties of the bionanocomposites may be related to the crystalline modulus and the size of brucite nanoplates as well as their surface area. Hence, reinforcement factors largely account for the mechanical performance of the bionanocomposites. At low concentrations of brucite, the enhancement in the tensile properties may be attributed to the high surface area and interfacial contact and the homogeneous dispersion of the nanoplates in the starch matrix. Increasing the amount of brucite effectively diminished the "true" surface area of the brucite nanoplates exposed because of greater agglomeration. Agglomeration tended to decrease the reinforcing effect of the brucite nanoplates thus resulting in the experimental and predicted reinforcement factors being similar. The decrease in mechanical strength for the highest volume fraction (7.5 wt.%) of brucite in the bionanocomposites was likely due to the greater amount of agglomerated brucite nanoplates that provided inferior reinforcement. The results from mechanical tests indicate that 1 wt.% brucite is a near optimal concentration to enhance the tensile properties of non-plasticized starch films.

3.4. Thermal behavior

Thermogravimetric analysis (TGA) was performed to evaluate the thermal stability of the bionanocomposites. The TG and DTG curves for pure starch film, pure brucite, and for films reinforced with 1 and 7.5 wt.% of brucite showed that samples were thermally stable up to 250 °C (Fig. 6). The mass loss below this temperature can be attributed to absorbed water release.

For pure starch film, two additional steps of mass loss occurred. The first step in the 277–350 °C range with a maximum temperature degradation rate (T_{max1}) at 301 °C corresponded to starch pyrolysis. This lead to the release of CO_2, CO, H_2O and other small volatile species, and formation of a carbonaceous residue (Greenwood, 1967; Zhang, Golding, & Burgar, 2002). The decomposition of this residue corresponded to the last step between 415 °C and 540 °C due to the oxidative atmospheric condition. A similar thermal profile was observed for the bionanocomposites, but it exhibited a visible displacement in T_{max1} with respect to that of pure starch film. The data of TGA (humidity content, T_{onset}, T_{max1} and inorganic content) have been collected as a function of brucite concentration in Table 1.

The moisture content of the various films was similar, approximately 10 wt.%. Moreover, a proportional relationship was observed between the inorganic content and brucite concentration in films. There was little difference in TGA parameters of samples filled with 0.25 wt.% or less of brucite compared to pure starch film. Nevertheless, for other bionanocomposites T_{onset} decreased to lower values, while T_{max1} slightly increased up to 310 °C for the bionanocomposite with 7.5 wt.% of brucite. Such minor but significant displacements indicates that brucite nanoplates could alter the thermal stability of starch films.

The flame retardancy property of brucite is very well described in the literature. The mechanism related to this effect is a based on the endothermic decomposition of brucite ($\Delta H = 1450\,J\,g^{-1}$), which occurs by release of structural water molecules (dehydroxylation) in a single event (Rothon & Hornsby, 1996). This reaction

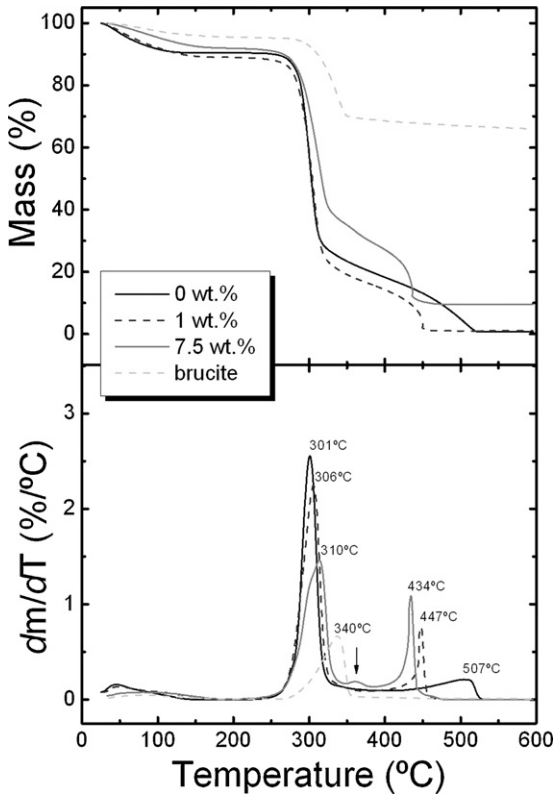

Fig. 6. Thermogravimetric analysis curves (thermogravimetric, upper; differential thermogravimetric, under) for the starch–brucite system. (Heating rate of 10 °C min^{-1} and atmosphere of synthetic air with flow of 60 mL min^{-1}.)

decreases the temperature in the vicinity of the brucite and retards the decomposition of the polymer matrix. As shown in Table 2, starch decomposes prior to brucite, but the overall decompositions occur at almost the same temperatures. It may be that increases in T_{max} occurred by the release of water from brucite within the starch matrix under decomposition. It is also important to consider that other mechanisms could have contributed to the increased T_{max} of starch, such as increased tortuosity in the diffusion pathway of pyrolysis gases due to the dispersion of the clay (Chiou et al., 2007), protective clay layer formation at the bionanocomposite surface (Chivrac et al., 2010), as well as starch–clay interactions (Chang et al., 2012). Nevertheless, another behavior was verified in TGA. For the highly incorporated bionanocomposites an additional step of mass loss was seen at T_{max1} close to 354–361 °C, with intensity proportional to brucite concentration (indicated by an arrow in DTG curve of 7.5 wt.% brucite incorporated film). If this event is ascribed to the decomposition of brucite detectible for highly incorporated bionanocomposites, then thermal stability of brucite nanoplates was also increased, and a protective effect between starch and brucite may be suspected.

To gain insight into the thermal behavior of the brucite–starch bionanocomposites, the 7.5 wt.% brucite incorporated film was submitted to combustion at temperatures of 350 °C (decomposition end for pure starch and brucite) and 600 °C (final TGA ramp), and the solid phases occurring in the calcined samples were identified by WAXS (results not shown). The corresponding WAXS pattern for the sample calcined at 600 °C was related only to magnesium oxide (MgO, periclase) (JCPDS indexation no. 45-0946), whereas an amorphous halo related to starch carbonaceous residue and

Table 1
TGA data of the brucite/starch bionanocomposites films.[a]

$Mg(OH)_2$ (wt.%)	H_2O (%)	T_{onset} (°C)[b]	T_{max1} (°C)	Inorganic (%)[c]
0.00	10.1 ± 0.6	277.5 ± 0.7	301.1 ± 0.1	0.53 ± 0.01
0.10	11.6 ± 0.8	274.7 ± 0.5	304.2 ± 0.2	0.55 ± 0.01
0.25	10.6 ± 1.3	273.1 ± 0.1	304.3 ± 0.4	0.63 ± 0.04
0.50	10.6 ± 0.4	272.5 ± 3.5	305.2 ± 1.2	0.70 ± 0.02
1.00	10.8 ± 0.4	273.5 ± 0.7	306.2 ± 0.2	1.10 ± 0.08
2.50	11.7 ± 1.6	271.9 ± 1.2	306.2 ± 0.3	2.40 ± 0.14
5.00	10.8 ± 0.3	272.5 ± 2.1	306.4 ± 0.5	3.15 ± 0.21
7.50	8.5 ± 1.2	273.0 ± 1.4	310.4 ± 4.2	7.25 ± 3.32
Pure brucite	4.5 ± 0.6	302.5 ± 0.7	337.3 ± 0.4	65.6 ± 0.57

[a] Average values from two replicates.
[b] Considered as the temperature at 3 wt.% mass loss of polymer.
[c] Determined by the residue left at 600 °C.

Table 2
Tensile mechanical properties of plasticized brucite–starch bionanocomposites.

Glycerol (wt.%)	Brucite (wt.%)	Brucite (vol.%[a])	E (MPa)	$E_{nanocomposite}/E_{matrix}$ (MPa)	ε_B (%)	σ_T (MPa)
10	0.00	0.00	556 ± 76	–	3.2 ± 1.3	20.2 ± 3.0
	0.10	0.06	620 ± 71	1.4	2.6 ± 1.0	18.1 ± 1.1
	0.25	0.16	803 ± 96	1.4	2.4 ± 0.7	16.4 ± 2.7
	0.50	0.31	1151 ± 101	2.1	2.9 ± 0.4	29.7 ± 1.9
	1.00	0.63	1459 ± 96	2.6	4.6 ± 1.1	32.0 ± 3.6
	2.50	1.55	1524 ± 101	2.7	5.0 ± 1.0	39.5 ± 3.8
	5.00	3.10	1361 ± 96	2.4	3.6 ± 0.8	35.1 ± 3.1
	7.50	4.65	691 ± 117	1.3	2.9 ± 0.9	24.7 ± 5.3
20	0.00	0.00	134 ± 5	–	23.6 ± 5.4	1.6 ± 0.4
	0.10	0.06	170 ± 69	0.8	17.5 ± 5.7	4.3 ± 1.0
	0.25	0.15	290 ± 30	2.2	16.0 ± 3.8	7.5 ± 1.5
	0.50	0.31	240 ± 34	1.8	12.2 ± 3.2	7.3 ± 0.7
	1.00	0.61	397 ± 90	2.9	8.1 ± 3.7	11.5 ± 1.3
	2.50	1.53	420 ± 75	3.1	9.1 ± 3.9	10.1 ± 1.5
	5.00	3.05	422 ± 77	3.1	13.8 ± 4.3	9.2 ± 1.6
	7.50	4.58	164 ± 42	1.2	15.0 ± 8.2	2.2 ± 1.0
30	0.00	0.00	28 ± 5	–	27.8 ± 4.3	2.0 ± 0.3
	0.10	0.06	22 ± 8	0.8	28.1 ± 3.1	2.6 ± 0.4
	0.25	0.15	22 ± 12	0.8	27.8 ± 5.2	1.4 ± 0.3
	0.50	0.30	19 ± 5	0.9	30.4 ± 4.9	1.5 ± 0.4
	1.00	0.60	22 ± 3	0.8	31.7 ± 3.0	2.1 ± 0.6
	2.50	1.50	39 ± 9	1.4	23.3 ± 5.8	3.0 ± 0.3
	5.00	3.00	81 ± 25	2.9	28.0 ± 5.1	4.0 ± 0.3
	7.50	4.50	62 ± 23	2.2	28.8 ± 5.7	3.4 ± 0.9

[a] Brucite volume fraction values were considered with basis on the density of the plasticized matrix (starch + glycerol mass basis). $\rho_{glycerol}$ = 1.26 g cm^{-3}.

scattering peaks mainly related to brucite were recognized for sample calcined at 350 °C. This means that brucite nanoplates persisted in the starch matrix even at higher temperature than those related to decomposition of pure components. A possible explanation for this behavior is that the carbonaceous product formed during starch decomposition acted as an insulating barrier, protecting the brucite nanoplates against heat, and increasing their thermal decomposition temperature. Hence, one may indicate a synergistic thermal effect between starch and brucite, once the thermal parameters of both components were displaced toward high values. A final behavior seen in TGA is that the thermal decomposition of the carbonaceous residue was displaced from 507 °C to lower T_{max} at 447 °C and 435 °C, for films containing 1 wt.% and 7.5% of brucite, respectively. This suggests that periclase own catalytic activity on the thermal decomposition of the starch carbonaceous product. The accurate description of the chemical mechanism involving the decomposition of brucite–starch bionanocomposites at high temperatures deserves further investigation.

3.5. Plasticized bionanocomposites

The influence of glycerol at contents of 10, 20 and 30 wt.% on the mechanical behavior of the brucite-reinforced starch bionanocomposites was examined. The tensile properties have been summarized in Table 2. The mechanical properties of the starch films were glycerol dependent as expected. Regarding the non-plasticized starch film (see Fig. 5), the elastic modulus and tensile strength decreased with only 10 wt.% of glycerol and were comparably low for the plasticizer contents of 20 wt.% and 30 wt.%. On the contrary, noticeable values of elongation at break (~28%) were observed with increasing plasticizer content. These results suggest that sufficient hydrogen bonds were formed between starch and glycerol, causing a fragile–ductile transition in the mechanical behavior of these films.

A clear reinforcing effect was observed for all contents of glycerol investigated. In the case of 10 wt.% glycerol plasticized bionanocomposites, the mechanical data showed that significant increases in tensile strength occurred just when the brucite concentration was 0.5 wt.% or higher when experimental error was taken into account. The modulus and strength gradually increased then decreased sharply at 7.5 wt.%, whereas elongation appeared independent of brucite concentration. Therefore, the mechanical behavior of these films was close to the non-plasticized bionanocomposites previously reported, probably due to the low amount of plasticizer incorporated in the samples.

A similar effect of brucite concentration on tensile properties was verified at the intermediate plasticizer content (20 wt.% glycerol). A reinforcing effect also occurred for these bionanocomposites, as demonstrated by the increases in the reinforcement factor and tensile strength. Nevertheless the ductility for this composition was affected more due to the incorporation of brucite. A reduction of almost 100% in the elongation at break values occurred for the 20 wt.% glycerol plasticized bionanocomposites containing 1 wt.% or more of brucite. At these concentrations, the starch–brucite interactions probably overlapped the starch–glycerol interactions, restricting the structural mobility and decreasing the deformation of the films. Again, the poorest mechanical performance was observed for the 7.5 wt.% brucite bionanocomposite.

Among all compositions investigated, only the 30 wt.% glycerol plasticized bionanocomposites showed a brucite-independent mechanical behavior. This may be related to the phase separation induced by high contents of glycerol (>27%), such that domains rich either in polymer or plasticizer are formed within the starch matrix (Lourdin, Coignard, Bizot, & Colonna, 1997). In the case of low brucite concentration, some nanoplates probably dispersed into the glycerol-rich domains, thus reducing their reinforcing efficiency. For these highly plasticized films, a significant reinforcing effect was observed only for brucite concentrations of 2.5 wt.%, 5 wt.% and 7.5 wt.% ($E_{nanocomposite}/E_{matrix} > 1$). Similar effect on the properties at fracture was observed where, for example an increase of almost 100% for tensile strength was observed at 5 wt.% of brucite. The elongation at break for these bionanocomposites was ~28% even at high concentrations of nanoplates.

4. Conclusion

A successful preparation of green bionanocomposites films based on starch as matrix and brucite nanoplates as nanofiller was reported in this study. Brucite nanoplates can be homogeneously dispersed inside of a starch matrix using the casting method when incorporated at low concentrations. An opposite morphology was verified at high brucite concentrations, in which the nanoplates formed agglomerates. Furthermore, a good filler-matrix adhesion was confirmed in the bionanocomposites, which was expected because of the hydrophilic nature of the phases.

The addition of brucite nanoplates at low concentrations enhanced the tensile strength and elastic modulus of the non-plasticized starch matrix. The homogeneous dispersion was fundamental to achieve high reinforcement. The interparticle agglomeration had a key influence on the interfacial area formed between the components of the bionanocomposites, reducing the mechanical reinforcement. These issues accounted for the disparity between the experimental reinforcement factors and theoretical ones calculated by the Halpin–Tsai model. As indicated by the tensile properties, the 1 wt.% brucite was the optimal concentration to enhance the mechanical properties of non-plasticized starch films, whereas 7.5 wt.% was an excessive concentration.

High brucite concentrations did not ensure improved mechanical properties but could be effective to enhance the thermal stability of the starch films. This was seen from increases ($\Delta T = 9$ °C) in the T_{max} of starch. Nevertheless, higher concentrations of brucite perhaps are necessary to cause a practical flame retardant effect on starch matrices. A protective thermal effect between starch and brucite was observed in the TGA and WAXS analyses.

Finally, investigation into the tensile properties of glycerol plasticized starch films demonstrated that the reinforcing effect of brucite nanoplates was high in a range of plasticizer content from 10 to 20 wt.%. The optimal range in brucite concentration was higher (2.5 wt.%) in 30 wt.% glycerol plasticized starch films. Regarding these plasticized bionanocomposites, further studies are needed to define an optimized composition in terms of mechanical and thermal properties, which are doubtless related not only to the content of glycerol, but also the size and morphology of the brucite nanoparticles.

This study demonstrated the potential of brucite nanoparticles to improve the properties of starch-based plastics. Since both biopolymer and nanoparticle are environmentally compatible and non-toxic components, the green bionanocomposites developed have potential for various purposes, especially for food contact and food packaging applications.

Acknowledgments

The authors are grateful to Embrapa, FINEP/MCT, CNPq, CAPES and Labex Embrapa/ARS for their financial support. The authors thank to Mr. Vitor Anibal do Sacramento Mendes from LCE/DEMA-UFSCar for his helpful assistance with the SEM characterizations and to Mr. Luiz Francisco de Mattêo Ferraz from CNPDIA for has carried out the WAXS measurements. F.K.V. Moreira is grateful to

FAPESP agency (Proc. no. 2010/11584-5) for his Ph.D. scholarship. This study is a part of the researches conducted by the Rede de Nanotecnologia Aplicada ao Agronegócio (Rede Agronano), Brazil.

References

An, D., Wang, L., Zheng, Y., Guan, S., Gao, X., Tian, Y., et al. (2009). In situ preparation and surface modification of magnesium hydroxide nanoparticles. *Colloids and Surfaces A*, *348*, 9–13.

Avérous, L. J. (2004). Biodegradable multiphase systems based on plasticized starch: A review. *Macromolecular Science Part C: Polymer Reviews*, *44*(3), 231–274.

Baranek, Ph., Lichanot, A., Orlando, R., & Dovesi, R. (2001). Structural and vibrational properties of solid $Mg(OH)_2$ and $Ca(OH)_2$ – Performance of various Hamiltonians. *Chemical Physics Letters*, *340*, 362–369.

Brucite Mineral Data. http://webmineral.com/data/Brucite.shtml. Accessed 07.17.12.

Carrado, K. A. (2004). Introduction: Clay structure, surface acidity, and catalysis. In S. M. Auerbach, K. A. Carrado, & P. K. Dutta (Eds.), *Handbook of layered materials* (pp. 1–39). New York: Marcel Dekker Inc.

Chiou, B.-S., Wood, D., Yee, E., Imam, S. H., Glenn, G. M., & Orts, W. J. (2007). Extruded starch–nanoclay nanocomposites: Effects of glycerol and nanoclay concentration. *Polymer Engineering and Science*, http://dx.doi.org/10.1002/pen.20903

Chang, P. R., Wu, D., Anderson, D. P., & Ma, X. (2012). Nanocomposites based on plasticized starch and rectorite clay: Structure and properties. *Carbohydrate Polymers*, *89*, 687–693.

Chen, B., & Evans, J. R. G. (2005). Thermoplastic starch–clay nanocomposites and their characteristics. *Carbohydrate Polymers*, *61*, 455–463.

Chivrac, F., Pollet, E., Schmutz, M., & Avérous, L. (2008). New approach to elaborate exfoliated starch-based nanobiocomposites. *Biomacromolecules*, *9*, 896–900.

Chivrac, F., Pollet, E., Schmutz, M., & Avérous, L. (2010). Starch nano-biocomposites based on needle-like sepiolite clays. *Carbohydrate Polymers*, *80*, 145–153.

Corradini, E., Lotti, C., De Medeiros, E. S., De Carvalho, A. J. F., Curvelo, A. A., & Mattoso, L. H. C. (2005). Estudo Comparativo de Amidos Termoplásticos Derivados do Milho com Diferentes Teores de Amilose. *Polímeros: Ciência e Tecnologia*, *15*(4), 268–273.

Darder, M., Aranda, P., & Ruiz-Hitzky, E. (2007). Bionanocomposites: A new concept of ecological, bioinspired, and functional hybrid materials. *Advanced Materials*, *19*, 1309–1319.

De Carvalho, A. J. F., Curvelo, A. A. S., & Agnelli, J. A. M. (2001). A first insight on composites of thermoplastic starch and kaolin. *Carbohydrate Polymers*, *45*, 189–194.

Ding, Y., Zhang, G., Wu, H., Hai, B., Wang, L., & Qian, Y. (2001). Nanoscale magnesium hydroxide and magnesium oxide powders: Control over size, shape, and structure via hydrothermal synthesis. *Chemistry of Materials*, *13*, 435–440.

Greenwood, C. T. (1967). The thermal degradation of starch. *Advances in Carbohydrate Chemistry and Biochemistry*, *22*, 483–515.

Halpin, J. C., & Kardos, J. L. (1972). Moduli of crystalline polymers employing composite theory. *Journal of Applied Physics*, *43*(5), 2235–2241.

Halpin, J. C., & Kardos, J. L. (1976). The Halpin–Tsai equations: A review. *Polymer Engineering and Science*, *16*, 344–352.

He, Y., Wang, J., Deng, H., Yin, Q., & Gong, J. (2008). Comparison of different methods to prepare MgO whiskers. *Ceramics International*, *34*, 1399–1403.

Henrist, C., Mathieu, J.-P., Vogels, C., Rulmont, A., & Cloots, R. J. (2003). Morphological study of magnesium hydroxide nanoparticles precipitated in dilute aqueous solution. *Journal of Crystal Growth*, *249*, 321–330.

Imam, S., Glenn, G., Chiou, B.-S., Shey, J. R., & Narayan, O. W. (2008). Types, production and assessment of biobased food packaging materials. In E. Chiellini (Ed.), *Environmentally compatible food packaging* (pp. 29–57). Cambridge: Woodhead Publishing Limited.

Jeevanandam, P., Mulukutla, R. S., Yang, Z., Kwen, H., & Klabunde, K. J. (2007). Nanocrystals to nanorods: A precursor approach for the synthesis of magnesium hydroxide nanorods from magnesium oxychloride nanorods starting from nanocrystalline magnesium oxide. *Chemistry of Materials*, *19*, 5395–5403.

Jia, B., & Gao, L. J. (2006). Morphology transformation of nanoscale magnesium hydroxide: From nanosheets to nanodisks. *American Ceramic Society*, *89*(12), 3881–3884.

Liu, H., Wang, R., & Xu, X. (2010). Thermal stability and flame retardancy of PET/magnesium salt composites. *Polymer Degradation and Stability*, *95*, 1466–1470.

Lourdin, D., Coignard, L., Bizot, H., & Colonna, P. (1997). Influence of equilibrium relative humidity and plasticizer concentration on the water content and glass transition of starch materials. *Polymer*, *38*(21), 5401–5406.

Lv, J., Qiu, L., & Qu Baojun, J. (2004). Controlled growth of three morphological structures of magnesium hydroxide nanoparticles by wet precipitation method. *Journal of Crystal Growth*, *267*, 676–684.

Mitrus, M. (2009). TPS and its nature. In L. P. B. M. Janssen, & L. Moscicki (Eds.), *Thermoplastic starch: A green material for various industries* (pp. 77–102). Germany: Wiley-VCH Verlag GmbH & Co. KGaA.

Norman, D. A., & Robertson, R. E. (2003). Rigid-particle toughening of glassy polymers. *Polymer*, *44*, 2351–2362.

Oyama, H. O., Sekikawa, M., & Ikezawa, Y. J. (2011). Influence of the polymer/inorganic filler interface on the mechanical, thermal, and flame retardant properties of polypropylene/magnesium hydroxide composites. *Macromolecular Science Part B: Physics*, *50*(3), 463–483.

Ray, S. S., & Bousmina, M. (2005). Biodegradable polymers and their layered silicate nanocomposites: In greening the 21st century materials world. *Progress in Materials Science*, *50*, 962–1079.

Rothon, R. N., & Hornsby, P. R. (1996). Flame retardant effects of magnesium hydroxide. *Polymer Degradation and Stability*, *54*, 383–385.

Utamapanya, S., Klabunde, K. J., & Schlup, J. R. (1991). Nanoscale metal oxide particles/clusters as chemical area magnesium hydroxide and magnesium oxide reagents. Synthesis and properties of ultrahigh surface. *Chemistry of Materials*, *3*, 175–181.

Van Soest, J. J. G., Hulleman, S. H. D., De Wit, D., & Vliegenthart, J. F. G. (1996). Crystallinity in starch bioplastics. *Industrial Crops and Products*, *5*, 11–22.

Wu, D., Chang, P. R., & Ma, X. (2011). Preparation and properties of layered double hydroxide–carboxymethylcellulose sodium/glycerol plasticized starch nanocomposites. *Carbohydrate Polymers*, *86*, 877–882.

Wilhelm, H.-M., Sierakowski, M.-R., Souza, G. P., & Wypych, F. (2003). The influence of layered compounds on the properties of starch/layered compound composites. *Polymer International*, *52*, 1035–1044.

Yan, C., Xue, D., Zou, L., Yan, X., & Wang, W. J. (2005). *Journal of Crystal Growth*, *282*, 448–454.

Xia, X., Weidner, D. J., & Zhao, H. (1998). Equation of state of brucite: Single-crystal Brillouin spectroscopy study and polycrystalline pressure–volume–temperature measurement. *American Mineralogist*, *83*, 68–74.

Zhang, X., Golding, J., & Burgar, I. (2002). Thermal decomposition chemistry of starch studied by ^{13}C high-resolution solid-state NMR spectroscopy. *Polymer*, *43*, 5791–5796.

Zhao, R., Torley, P., & Halley, P. J. (2008). Emerging biodegradable materials: Starch- and protein-based bio-nanocomposites. *Journal of Materials Science*, *43*, 3058–3071.

Zhao, W. B. (1998). Starch. In J. E. Mark (Ed.), *Polymer data handbook* (pp. 975–979). Oxford: Oxford University Press Inc.

Zhuo, L., Ge, J., Cao, L., & Tang, B. (2009). Solvothermal synthesis of CoO, Co_3O_4, $Ni(OH)_2$ and $Mg(OH)_2$ nanotubes. *Crystal Growth and Design*, *6*(1), 1–6.